Anthropogenic emissions of NO_x over China: Reconciling the difference of inverse modeling results using GOME-2 and OMI measurements

Dasa Gu[1], Yuhang Wang[1], Charles Smeltzer[1], and K. Folkert Boersma[2,3]

[1]School of Earth and Atmospheric Sciences, Georgia Institute of Technology, Atlanta, Georgia, USA, [2]Climate Observations Department, Royal Netherlands Meteorological Institute, De Bilt, Netherlands, [3]Department of Meteorology and Air Quality, Wageningen University, Wageningen, Netherlands

Abstract Inverse modeling using satellite observations of nitrogen dioxide (NO_2) columns has been extensively used to estimate nitrogen oxides (NO_x) emissions in China. Recently, the Global Ozone Monitoring Experiment-2 (GOME-2) and Ozone Monitoring Instrument (OMI) provide independent global NO_2 column measurements on a nearly daily basis at around 9:30 and 13:30 local time across the equator, respectively. Anthropogenic NO_x emission estimates by applying previously developed monthly inversion (MI) or daily inversion (DI) methods to these two sets of measurements show substantial differences. We improve the DI method by conducting model simulation, satellite retrieval, and inverse modeling sequentially on a daily basis. After each inversion, we update anthropogenic NO_x emissions in the model simulation with the newly obtained a posteriori results. Consequently, the inversion-optimized emissions are used to compute the a priori NO_2 profiles for satellite retrievals. As such, the a priori profiles used in satellite retrievals are now coupled to inverse modeling results. The improved procedure was applied to GOME-2 and OMI NO_2 measurements in 2011. The new daily retrieval-inversion (DRI) method estimates an average NO_x emission of 6.9 Tg N/yr over China, and the difference between using GOME-2 and OMI measurements is 0.4 Tg N/yr, which is significantly smaller than the difference of 1.3 Tg N/yr using the previous DI method. Using the more consistent DRI inversion results, we find that anthropogenic NO_x emissions tend to be higher in winter and summer than spring (and possibly fall) and the weekday-to-weekend emission ratio tends to increase with NO_x emission in China.

1. Introduction

Nitrogen oxides ($NO_x = NO + NO_2$) play a key role in the formation of ozone and secondary aerosols. NO_x is emitted from both anthropogenic sources (e.g., fossil fuel combustion and human-induced biomass burning) and natural sources (e.g., lightning, wildfires, and soil emissions). One region that has witnessed rapid changes in NO_x emissions in the past two decades is China. These changes have been reported previously in analyses of satellite-measured tropospheric nitrogen dioxide (NO_2) columns [e.g., *Ghude et al.*, 2009; *Gu et al.*, 2013; *Ma et al.*, 2006; *Richter et al.*, 2004; *Uno et al.*, 2007; *van der A et al.*, 2006].

The traditional bottom-up inventories of NO_x emissions, estimated from limited information of emission source factors and statistical data over China, could have large uncertainties [e.g., *Ohara et al.*, 2007; *Streets et al.*, 2003]. On the basis of the relationship between local emission and tropospheric NO_2 column simulated by a chemical transport model, inverse modeling has been used to combine bottom-up inventories with top-down constraints from satellite column NO_2 observations, such as Global Ozone Monitoring Experiment (GOME), Scanning Imaging Absorption Spectrometer for Atmospheric Chartography (SCIAMACHY), Ozone Monitoring Instrument (OMI), and Global Ozone Monitoring Experiment-2 (GOME-2), in order to reduce uncertainties in NO_x emission estimations [e.g., *Choi et al.*, 2012; *Han et al.*, 2009; *He et al.*, 2007; *Kunhikrishnan et al.*, 2004; *Kurokawa et al.*, 2009; *Lin et al.*, 2012; *Martin et al.*, 2003; *Richter et al.*, 2005; *Shi et al.*, 2008; *Stavrakou et al.*, 2008; *Zhang et al.*, 2012].

Martin et al. [2003] developed the first monthly inversion (MI) method by combining the bottom-up emission inventory with top-down constraints from GOME NO_2 column measurements. The method was extended by *Zhao and Wang* [2009] to carry out the emission inversion iteratively on a daily basis to account in part for the nonlinear effects in chemical feedbacks. One issue that has not been discussed extensively is that the inverse modeling that results from different satellites can differ significantly; part of the issue is attributable to a priori profiles used in retrievals [e.g., *Irie et al.*, 2012; *Lin et al.*, 2010; *Vinken et al.*, 2014]. We choose to use
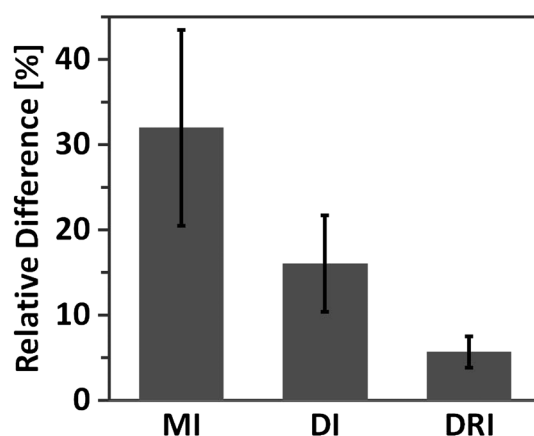
Figure 1. Relative difference between GOME-2 and OMI measurement constrained anthropogenic NO_x emission estimates over China using MI [*Martin et al.*, 2003], DI [*Zhao and Wang*, 2009], and improved DRI methods for 2011. The vertical bar shows 1σ uncertainty.

GOME-2 and OMI measurements in this study because these two instruments have a similar temporal sampling frequency that is substantially better than SCIAMACHY. Figure 1 compares the inverse modeling results of anthropogenic NO_x emissions between using GOME-2 and OMI measurements. Satellite measurements, a priori emissions, and the regional chemical and transport model used in the comparison will be discussed in the next section. By applying the MI method [*Martin et al.*, 2003] with simulations from the Regional Chemical and Transport Model (REAM), we find that the relative difference of NO_x inversion emission estimates between using GOME-2 and OMI measurements is $32 \pm 12\%$ over China in 2011. The difference is reduced to $16 \pm 6\%$ by using the daily inversion (DI) method [*Zhao and Wang*, 2009], but it remains very large.

The substantial difference of inverse modeling results from the two sets of satellite measurements raises an obvious question of consistency in potential science applications of these emission estimates. While not solving the problem, the iteration in the DI method helps reduce the difference compared to MI method. In this study, we examine if the difference can be further reduced by improving the inverse modeling method. We improve the DI method by updating on a daily basis anthropogenic NO_x emissions in REAM using the inversion results and subsequently the a priori NO_x profiles used in the satellite retrieval. The improved daily retrieval-inversion (DRI) method therefore couples the retrieval profiles to inverse modeling results and ensures the consistency between them. The DRI method is applied in the REAM model to improve surface anthropogenic NO_x emission estimates with GOME-2 and OMI measurements over China in 2011. The DRI inversion results are compared to those using the DI method to demonstrate the benefits of the new method. We analyze further the seasonal and weekday-to-weekend variations of anthropogenic NO_x emissions over China using the new DRI inversion products.

2. Satellite Observations and Inverse Modeling Methods

2.1. GOME-2 and OMI Tropospheric NO_2 Columns

Both GOME-2 and OMI instruments are nadir-viewing spectrometers [e.g., *Boersma et al.*, 2004, 2007, 2011]. The OMI instrument was launched onboard the Aura satellite in July 2004, and it has a spatial resolution of 24×13 km^2 at nadir [*Levelt et al.*, 2006]. The GOME-2 instrument was launched onboard the METOP-A satellite in October 2006 with ground pixel size of 80×40 km^2 [*Irie et al.*, 2012]. The local equator crossing time is around 9:30 for GOME-2 and around 13:30 for OMI. We excluded the data in all flagged rows with anomalies for the OMI measurements (http://www.knmi.nl/omi/research/product/rowanomaly-background.php). In addition, we only use measured NO_2 column data when cloud fraction is $< 30\%$ for both instruments.

In MI and DI inversions, we use the Royal Netherlands Meteorological Institute (KNMI) OMI (DOMINO2 v2.0) and GOME-2 (TM4NO2A v2.3) tropospheric NO_2 vertical column density (VCD) products [*Boersma et al.*, 2004, 2007]. Comparing these two products, the GOME-2 VCDs are significantly higher than OMI VCDs up to $>110\%$ over eastern China in 2011 (Figure S1 in the supporting information). Higher GOME-2 VCD values reflect a longer chemical lifetime of NO_x in midmorning than the OMI observation time of early afternoon [e.g., *Irie et al.*, 2012].

In the DRI method, we recompute tropospheric NO_2 VCD data using OMI or GOME-2 measurements. In order to maintain consistency in comparison, we use the KNMI algorithm in the retrievals of both OMI and GOME-2 tropospheric NO_2 VCDs [*Boersma et al.*, 2011]. The retrieval procedure includes estimation of NO_2 slant column density (SCD), calculation of tropospheric SCD by subtracting the TM4 assimilated stratospheric column, and converting the tropospheric SCD into VCD with the tropospheric air mass factor (AMF). The tropospheric AMF
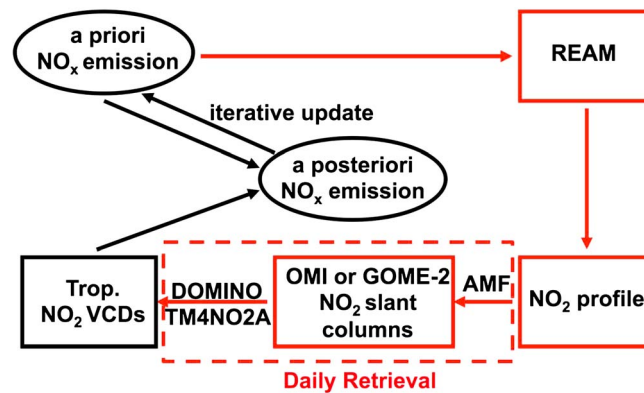
Figure 2. Schematic diagrams of the DI (in black arrows) and new DRI (in red arrows) methods. In the DRI method, the daily iterative update includes NO_x emissions, NO_2 profiles, and tropospheric NO_2 VCD retrievals. In the DI method, only NO_x emissions are updated daily. In the DRI method, satellite NO_2 SCD products are used; In the DI method, KNMI DOMINO2 and TM4NO2A tropospheric NO_2 VCD products are used.

calculation depends on a priori tropospheric NO_2 profile, surface albedo, cloud pressure, cloud fraction, and satellite-viewing geometry. A more detailed description can be found in *Boersma et al.* [2007]. In the MI and DI methods [*Martin et al.*, 2003; *Zhao and Wang*, 2009], the model simulation of a priori tropospheric profiles is decoupled from inverse modeling. In other words, the emissions used in the model and retrieval are not necessarily consistent with the inverse modeling results. We solve this problem in the DRI method by updating the model emissions and the a priori profiles using inverse modeling results on a daily basis (to be shown in Figure 2).

The error in the retrieval of NO_2 tropospheric VCD is determined by those in total SCD, stratospheric SCD, and tropospheric AMF estimation. In this study, we use total and stratospheric SCD errors from KNMI DOMINO2 and TM4NO2A products and compute the error of tropospheric AMF estimation following the KNMI algorithm. The details of error analysis were described by *Boersma et al.* [2004, 2007, 2011] and *Hains et al.* [2010]. In general, the errors of total and stratospheric SCD estimations are relatively small ($<0.7 \times 10^{15}$ molecules cm^{-2}) relative to high tropospheric VCDs ($>10 \times 10^{15}$ molecules cm^{-2}) over eastern China [*Zhao and Wang*, 2009]. The error in tropospheric AMF comes from surface albedo, cloud fraction, cloud pressure, and profile shape. The total error per retrieval is ~30% over most areas in China for both OMI and GOME-2.

2.2. REAM Model

The 3-D REAM has been applied in a number of tropospheric chemistry and transport studies over East Asia, North America, and polar regions [e.g., *Choi et al.*, 2005, 2008a, 2008b; *Jing et al.*, 2006; *Liu et al.*, 2010, 2012a, 2012b; *Wang et al.*, 2006, 2007; *Yang et al.*, 2011; *Zeng et al.*, 2003, 2006; *Zhao and Wang*, 2009; *Zhao et al.*, 2009a, 2009b, 2010]. The model has a horizontal resolution of 70×70 km^2 with 21 vertical layers in the troposphere. Transport is driven by Weather Research and Forecasting (WRF) model assimilated meteorological fields constrained by the National Centers for Environmental Prediction (NCEP) reanalysis products (http://www.esrl.noaa.gov/psd/). The chemistry mechanism in REAM is adopted from the GEOS-Chem model [*Bey et al.*, 2001] with updates of kinetics data (http://jpldataeval.jpl.nasa.gov/). The anthropogenic NO_x and VOCs emissions are from *Zhang et al.* [2009]. The biomass burning emissions are taken from the Global Fire Emissions Database, Version 2 (GFEDv2.1) (available at http://daac.ornl.gov/). The lightning NO_x emission is parameterized by *Zhao et al.* [2010].

2.3. Inverse Modeling

The MI method for anthropogenic NO_x emissions and uncertainties based on bottom-up and top-down constraints was developed by *Martin et al.* [2003]. We compared the emission estimates by using the DI method [*Zhao and Wang*, 2009] with that using the MI method based on KNMI DOMINO2 and TM4NO2A products in Figure 1. The improvement in annualized difference from 32% (MI) to 16% (DI) is significant. However, the difference in the DI method can still reach to >32% on a monthly basis (to be shown in Figure 4).

In the DI method, only NO_x emission is computed iteratively on a daily basis (Figure 2). In this method, which largely follows *Martin et al.* [2003], a top-down emission is estimated by scaling the a priori emission with the ratio of observed and simulated tropospheric NO_2 column. The a posteriori emission is then calculated by error-weighted averaging of the a priori and top-down emissions (the error distributions of the a priori NO_x and the top-down NO_x estimates are assumed to be lognormal). The optimized a posteriori emission and its errors are then used as the a priori in the next day. The whole process iterates daily at the satellite overpass time.

One potential problem in the DI method is that the vertical profiles used in the retrieval are not necessarily consistent with the a posteriori emissions. For example, an increase of emissions will generally increase the
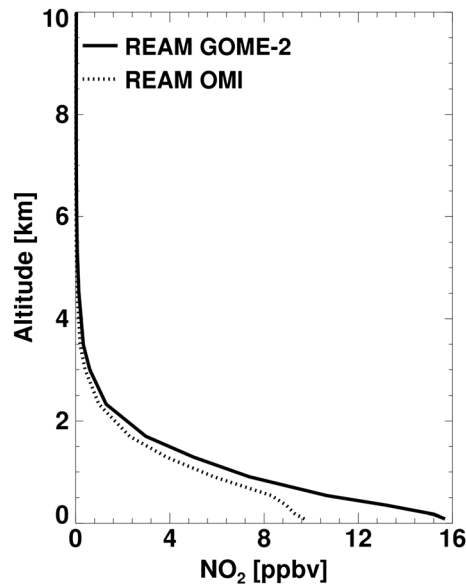
Figure 3. Simulated monthly mean NO_2 vertical profiles over Bijing in the DRI method at GOME-2 and OMI local overpass times for March 2011.

vertical gradient of NO_2 profiles and change the AMF values used in the retrieval of tropospheric NO_2 column (section 2.1). Furthermore, when we compare the inverse modeling results from two satellite measurements, additional inconsistency can be introduced if the model used to compute NO_2 profiles in AMF calculation is different from the model used in inverse modeling. Figure 3 shows REAM-simulated monthly mean NO_2 profiles at GOME-2 and OMI overpass times for March, which has the largest monthly mean difference between DI inversion results using KNMI DOMINO2 OMI and TM4NO2A GOME-2 tropospheric NO_2 VCD products for 2011 (to be shown in Figure 4). The vertical gradient of NO_2 in the lower troposphere is greater for GOME-2 than OMI since GOME-2 overpass is in midmorning while OMI overpass is in early afternoon. We did not show in the figure the corresponding profiles from TM4, which are used in the KNMI products, since the TM4 profiles for GOME-2 retrievals were not archived.

In the DRI method, we improve NO_x inverse modeling by updating the emissions from the inversion results and subsequently the a priori NO_2 profiles used in the satellite retrieval on a daily basis (Figure 2). Tropospheric NO_2 columns are retrieved online daily before inverse modeling. Tropospheric AMFs are first computed with REAM-simulated NO_2 profiles and then used in retrieval process to derive tropospheric NO_2 VCD from GOME-2 or OMI NO_2 SCD. The online-computed tropospheric NO_2 VCD is subsequently applied in inverse modeling to estimate the a posteriori emissions and errors. After the inversion, the optimized a posteriori emissions and errors are then used as the a priori data in subsequent model simulation, satellite retrieval, and inverse modeling. Therefore, we ensure consistency between the a posteriori emissions and the NO_2 profiles used in GOME-2 and OMI retrievals.

The uncertainties of the a posteriori emissions are derived from those in a priori and top-down emission estimates. Uncertainties in top-down emission estimates come from those in tropospheric NO_2 VCD retrievals and model simulations. The retrieval error is discussed in section 2.1. The uncertainty of model simulation is estimated at 30% and that of the bottom-up inventory is ~60% over China [*Zhao and Wang*, 2009]. The overall uncertainties of the a posteriori emission are typically in the range of 20–40% over polluted eastern China (Figure S2 in the supporting information).
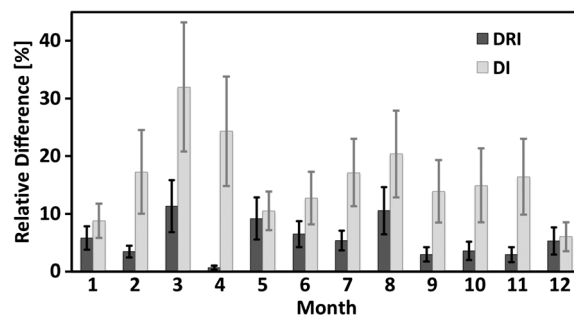

Figure 4. Relative differences of monthly anthropogenic NO_x emission estimates over China between GOME-2 and OMI measurement-based inversion results using DRI (black) and DI (grey) methods for 2011. The vertical bars show 1σ uncertainty.

3. Results and Discussions

3.1. Comparison Between GOME-2 and OMI Measurement Based Inversion Results

We showed in Figure 1 the yearly relative difference between GOME-2 and OMI measurement based inversion results for NO_x emissions over China using the MI and DI methods, respectively. The DI method reduces the annual mean NO_x emission difference between OMI and GOME-2 based inversion results to $16 \pm 6\%$ from $32 \pm 12\%$ of the MI method. However, the monthly difference is still quite large in DI method, ranging from <10% in December and

January to > 30% in March (Figure 4). The newly developed DRI method, on the other hand, reduces the difference consistently every month compared to the DI method. The maximum difference, which is in March, is reduced to < 12%. The annual mean difference decreases to $5 \pm 2\%$.

Figure S1 in the supporting information compares tropospheric NO_2 VCDs between KNMI DOMINO2 OMI and TM4NO2A GOME-2 products and those retrieved by DRI. While the chemical lifetime difference reflected in part in the difference between NO_2 vertical profiles at GOME-2 and OMI observation times (Figure 3) and it is expected to yield higher NO_2 VCDs at GOME-2 observation time than OMI, the column difference is clearly much larger between KNMI DOMINO2 OMI and TM4NO2A GOME-2 products than between the corresponding DRI retrievals. A close inspection reveals that the differences between KNMI and DRI tropospheric VCDs are much larger for GOME-2 than OMI. The main reason is that KNMI GOME-2 tropospheric VCD estimates are much larger than DRI results. The difference between KNMI and DRI OMI products is much smaller in comparison. Since the TM4 profiles used in KNMI GOME-2 retrievals were not archived, we cannot compare TM4 profiles to those from REAM.

While the total a posteriori emissions over China in the DRI method are in good agreement between using OMI and GOME-2 measurements, regional differences still exist. Figure 5 (top row) shows the annual mean a posteriori NO_x emissions over China for 2011 by using DRI method with GOME-2 measurements. There are high NO_x emissions in economically developed eastern and southern China. Comparing the a posteriori NO_x emissions from the two satellites, we find much larger differences in a posteriori NO_x emission estimates by using the DI method than the DRI method, especially over polluted eastern China (Figure S3 in the supporting information). As shown in Figure 5 (top row), the a posteriori NO_x emission estimates are significantly higher with GOME-2 than OMI measurements (20–60% over high-emission regions) when the DI method is applied. In comparison, the difference are significantly lower (0–20% over high-emission regions) when the DRI method is applied. The large positive bias of GOME-2 over OMI based estimates is much reduced.

The average a posteriori anthropogenic NO_x emission over China is 6.9 Tg N/yr with the DRI method, and the difference between using GOME-2 and OMI measurements is 0.4 Tg N/yr. In comparison, the OMI and GOME-2 difference between using the DI method with KNMI DOMINO2 and TM4NO2A products is significantly larger at 1.3 Tg N/yr. Considering the uncertainties in satellite measurements, retrieval, and model simulations, these results suggest that the inversion results using the measurements of OMI and GOME-2 are highly consistent when the DRI method is applied in inverse modeling.

In Figure 5 (bottom row), we compared simulated daytime tropospheric NO_2 VCDs by the DRI and DI methods with GOME-2 and OMI measurements. Simulated tropospheric NO_2 VCDs are similar to the spatial distribution of satellite-retrieved VCDs over China. More importantly, simulated daytime tropospheric NO_2 columns show much smaller differences between OMI and GOME-2 based results by using the DRI than DI method. On average, the simulated column difference decreased from 30% to 7% over eastern China. The high column bias of GOME-2 based results compared to those of OMI is much smaller in the DRI than DI method.

3.2. Seasonal Variation of Surface Anthropogenic NO_x Emissions in China

Figure 6 shows the monthly surface anthropogenic NO_x emission estimates using the DI and DRI methods with OMI and GOME-2 measurements. The relative differences between the two satellite data based emissions using DI and DRI methods have been shown in Figure 4. As shown in Figure 5, the a posteriori emission estimates using the DI method with GOME-2 measurements are noticeably higher than those with OMI measurements. The newly developed DRI method, on the other hand, gives fairly consistent emission estimates with GOME-2 and OMI measurements, well within the a posteriori uncertainties.

The seasonal variation of anthropogenic NO_x emissions has been investigated previously using satellite NO_2 measurements [e.g., *Jaegle et al.*, 2005; *Miyazaki et al.*, 2012]. The DRI emission estimates with GOME-2 and OMI measurements show similar seasonal variations (Figure 6). The largest variation is seen in February compared to January and May. The decrease of emissions in February is likely associated with the Chinese New Year holidays. Lower emissions in March to May probably reflect the lower energy consumption associated with transition of heating in winter and cooling in summer. A decrease of emissions to a lesser degree is seen in September and October probably for similar reasons as in spring, although this decrease is masked by the uncertainty of emission estimate. A longer term inverse modeling study is necessary to investigate if the spring and fall decrease pattern persists from year to year. We note here that the significant
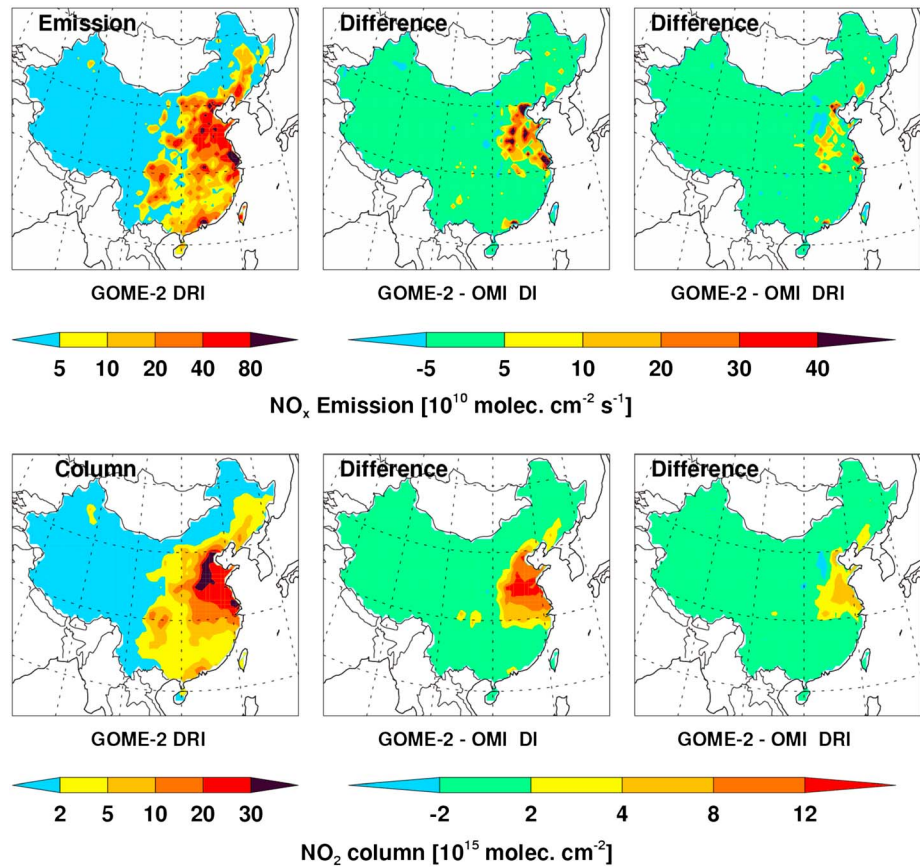
Figure 5. (top row) Annual mean a posteriori NO$_x$ emission estimates by using the (top, left) DRI method with GOME-2 measurements, and the differences of annual mean a posteriori NO$_x$ emission estimates between using GOME-2 and OMI measurements by using the (top, middle) DI and (top, right) DRI methods, over China for 2011. (bottom row) Annual mean simulated daytime tropospheric NO$_2$ VCDs by using (bottom, left) GOME-2 measurements, and the difference of simulated annual mean daytime tropospheric NO$_2$ VCDs between using GOME-2 and OMI measurement based emission estimates by the (bottom, middle) DI and (bottom, right) DRI methods, over China for 2011.

reduction of emission estimate difference in spring and fall using the DRI than DI method (Figure 4) is critical for discerning the seasonal change of emissions based on satellite measurements. The seasonal pattern of high emissions in winter and low emissions in spring are similar to the bottom-up estimate by *Zhang et al.* [2007], but the emission ratio of 1.4 of December and January to April and May found in this work is higher than that study.
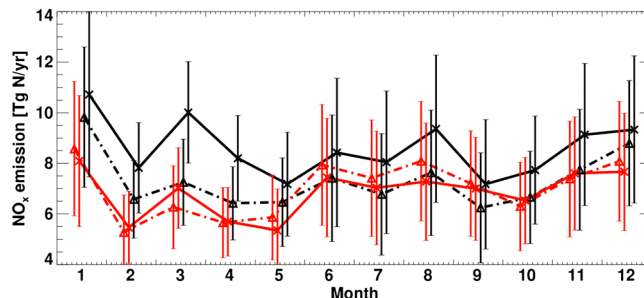

Figure 6. Monthly anthropogenic NO$_x$ emissions estimates by the DRI (red lines) and DI (black lines) methods with OMI (triangles, dashed lines) and GOME-2 (crosses, solid lines) measurements over China for 2011. The vertical bars show 1σ uncertainties.
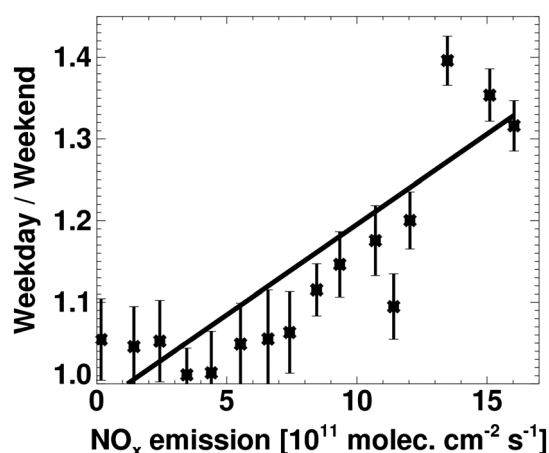
Figure 7. Weekday (Monday–Friday) to weekend (Saturday and Sunday) ratio of anthropogenic NO_x emissions as a function of NO_x emission rate over China for 2011. A vertical bar shows the 1σ uncertainty within each emission bin of 10^{11} molecules $cm^{-2} s^{-1}$. A least squares regression is shown by the black line.

3.3. Weekday to Weekend Emission Ratios

A significant weekly cycle of satellite observed NO_2 columns with a minimum value in weekend was found in urban regions in the USA, Europe, the Middle East, and Japan [e.g., *Beirle et al.*, 2003; *Boersma et al.*, 2009; *Choi et al.*, 2012; *Kaynak et al.*, 2009]. In contrast, no clear weekend effect was found in cities of China from satellite measurements [*Beirle et al.*, 2003; *Hayn et al.*, 2009]. In our analysis, we find a clearer weekday (Monday-Friday) to weekend (Saturday and Sunday) change signal using the inverse modeling results from the DRI method compared to the DI method with both GOME-2 and OMI measurements. In particular, the weekday to weekend emission ratio tends to be higher over high emission regions. We show the increase of this ratio with anthropogenic NO_x emission in Figure 7. The ratio is up to the range of 1.3–1.4, which is similar to a ratio of 1.2–1.5 in urban regions of the U.S. and Europe given in previous studies [*Beirle et al.*, 2003; *Choi et al.*, 2012; *Hayn et al.*, 2009; *Kaynak et al.*, 2009]. For regions with NO_x emissions $< 8 \times 10^{11}$ molecules $cm^{-2} s^{-1}$, the weekday to weekend emission ratio is close to 1, in agreement with previous analyses.

4. Conclusions

We improve the daily inversion of NO_x emissions by updating the emissions with the inversion results and subsequently the a priori NO_2 profiles used in satellite retrieval on a daily basis. The newly developed DRI method therefore ensures consistency between NO_x emission estimates and the NO_2 profiles used in satellite retrievals in a single modeling framework. We applied the methods to inverse modeling of anthropogenic NO_x emissions over China using GOME-2 and OMI NO_2 column measurements in 2011. The high bias of GOME-2 based emission estimates relative to those based on OMI measurements in the DI method is largely removed in the DRI method. The DRI method significantly reduces the difference of anthropogenic NO_x emission estimates between GOME-2 and OMI data based inversions to 0.3 Tg N/yr from 1.3 Tg N/yr using the DI method. The average emission rate of anthropogenic NO_x is 6.9 Tg/yr over China in 2011. We examine the seasonal and weekly anthropogenic NO_x emission variations in China using the DRI emission estimates. Anthropogenic NO_x emissions are lower in spring (possibly in the fall) than winter and summer. The emission ratio from December and January to April and May is 1.4, while the peak winter and summer month emissions are similar. The weekday to weekend emission ratio tends to increase with NO_x emissions, to the range of 1.3–1.4 in high NO_x emission regions, similar to those previously found in urban regions of the U.S. and Europe. In low and moderate emission regions ($< 8 \times 10^{11}$ molecules $cm^{-2} s^{-1}$), the weekday to weekend emission ratio is close to 1.

References

Beirle, S., U. Platt, M. Wenig, and T. Wagner (2003), Weekly cycle of NO_2 by GOME measurements: A signature of anthropogenic sources, *Atmos. Chem. Phys.*, 3, 2225–2232.
Bey, I., D. J. Jacob, R. M. Yantosca, J. A. Logan, B. D. Field, A. M. Fiore, Q. B. Li, H. G. Y. Liu, L. J. Mickley, and M. G. Schultz (2001), Global modeling of tropospheric chemistry with assimilated meteorology: Model description and evaluation, *J. Geophys. Res.*, 106(D19), 23,073–23,095, doi:10.1029/2001JD000807.
Boersma, K. F., H. J. Eskes, and E. J. Brinksma (2004), Error analysis for tropospheric NO_2 retrieval from space, *J. Geophys. Res.*, 109, D04311, doi:10.1029/2003JD003962.
Boersma, K. F., et al. (2007), Near-real time retrieval of tropospheric NO_2 from OMI, *Atmos. Chem. Phys.*, 7(8), 2103–2118.
Boersma, K. F., D. J. Jacob, M. Trainic, Y. Rudich, I. DeSmedt, R. Dirksen, and H. J. Eskes (2009), Validation of urban NO_2 concentrations and their diurnal and seasonal variations observed from the SCIAMACHY and OMI sensors using in situ surface measurements in Israeli cities, *Atmos. Chem. Phys.*, 9(12), 3867–3879.
Boersma, K. F., et al. (2011), An improved tropospheric NO_2 column retrieval algorithm for the ozone monitoring instrument, *Atmos. Meas. Tech.*, 4(9), 1905–1928.

Choi, Y., Y. H. Wang, T. Zeng, R. V. Martin, T. P. Kurosu, and K. Chance (2005), Evidence of lightning NO_x and convective transport of pollutants in satellite observations over North America, *Geophys. Res. Lett.*, *32*, L02805, doi:10.1029/2004GL021436.

Choi, Y., Y. Wang, T. Zeng, D. Cunnold, E. S. Yang, R. Martin, K. Chance, V. Thouret, and E. Edgerton (2008a), Springtime transitions of NO_2, CO, and O_3 over North America: Model evaluation and analysis, *J. Geophys. Res.*, *113*, D20311, doi:10.1029/2007JD009632.

Choi, Y., Y. H. Wang, Q. Yang, D. Cunnold, T. Zeng, C. Shim, M. Luo, A. Eldering, E. Bucsela, and J. Gleason (2008b), Spring to summer northward migration of high O_3 over the western North Atlantic, *Geophys. Res. Lett.*, *35*, L04818, doi:10.1029/2007GL032276.

Choi, Y., H. Kim, D. Tong, and P. Lee (2012), Summertime weekly cycles of observed and modeled NO_x and O_3 concentrations as a function of satellite-derived ozone production sensitivity and land use types over the Continental United States, *Atmos. Chem. Phys.*, *12*(14), 6291–6307.

Ghude, S. D., R. J. Van der A, G. Beig, S. Fadnavis, and S. D. Polade (2009), Satellite derived trends in NO_2 over the major global hotspot regions during the past decade and their inter-comparison, *Environ. Pollut.*, *157*(6), 1873–1878.

Gu, D., Y. Wang, C. Smeltzer, and Z. Liu (2013), Reduction in NO_x emission trends over China: Regional and seasonal variations, *Environ. Sci. Technol.*, *47*(22), 12,912–12,919.

Hains, J. C., et al. (2010), Testing and improving OMI DOMINO tropospheric NO_2 using observations from the DANDELIONS and INTEX-B validation campaigns, *J. Geophys. Res.*, *115*, D05301, doi:10.1029/2009JD012399.

Han, K. M., C. H. Song, H. J. Ahn, R. S. Park, J. H. Woo, C. K. Lee, A. Richter, J. P. Burrows, J. Y. Kim, and J. H. Hong (2009), Investigation of NO_x emissions and NO_x-related chemistry in East Asia using CMAQ-predicted and GOME-derived NO_2 columns, *Atmos. Chem. Phys.*, *9*(3), 1017–1036.

Hayn, M., S. Beirle, F. A. Hamprecht, U. Platt, B. H. Menze, and T. Wagner (2009), Analysing spatio-temporal patterns of the global NO_2-distribution retrieved from GOME satellite observations using a generalized additive model, *Atmos. Chem. Phys.*, *9*(17), 6459–6477.

He, Y., I. Uno, Z. Wang, T. Ohara, N. Sugirnoto, A. Shimizu, A. Richter, and J. P. Burrows (2007), Variations of the increasing trend of tropospheric NO_2 over central east China during the past decade, *Atmos. Environ.*, *41*(23), 4865–4876.

Irie, H., K. F. Boersma, Y. Kanaya, H. Takashima, X. Pan, and Z. F. Wang (2012), Quantitative bias estimates for tropospheric NO_2 columns retrieved from SCIAMACHY, OMI, and GOME-2 using a common standard for East Asia, *Atmos. Meas. Tech.*, *5*(10), 2403–2411.

Jaegle, L., L. Steinberger, R. V. Martin, and K. Chance (2005), Global partitioning of NO_x sources using satellite observations: Relative roles of fossil fuel combustion, biomass burning and soil emissions, *Faraday Discuss.*, *130*, 407–423.

Jing, P., D. Cunnold, Y. Choi, and Y. Wang (2006), Summertime tropospheric ozone columns from Aura OMI/MLS measurements versus regional model results over the United States, *Geophys. Res. Lett.*, *33*, L17817, doi:10.1029/2006GL026473.

Kaynak, B., Y. Hu, R. V. Martin, C. E. Sioris, and A. G. Russell (2009), Comparison of weekly cycle of NO_2 satellite retrievals and NO_x emission inventories for the continental United States, *J. Geophys. Res.*, *114*, D05302, doi:10.1029/2008JD010714.

Kunhikrishnan, T., M. G. Lawrence, R. von Kuhlmann, A. Richter, A. Ladstatter-Weissenmayer, and J. P. Burrows (2004), Analysis of tropospheric NO_x over Asia using the model of atmospheric transport and chemistry (MATCH-MPIC) and GOME-satellite observations, *Atmos. Environ.*, *38*(4), 581–596.

Kurokawa, J., K. Yumimoto, I. Uno, and T. Ohara (2009), Adjoint inverse modeling of NO_x emissions over eastern China using satellite observations of NO_2 vertical column densities, *Atmos. Environ.*, *43*(11), 1878–1887.

Levelt, P. F., E. Hilsenrath, G. W. Leppelmeier, G. H. J. van den Oord, P. K. Bhartia, J. Tamminen, J. F. de Haan, and J. P. Veefkind (2006), Science objectives of the ozone monitoring instrument, *IEEE Trans. Geosci. Remote Sens.*, *44*(5), 1199–1208.

Lin, J. T., M. B. McElroy, and K. F. Boersma (2010), Constraint of anthropogenic NO_x emissions in China from different sectors: A new methodology using multiple satellite retrievals, *Atmos. Chem. Phys.*, *10*(1), 63–78.

Lin, J. T., Z. Liu, Q. Zhang, H. Liu, J. Mao, and G. Zhuang (2012), Modeling uncertainties for tropospheric nitrogen dioxide columns affecting satellite-based inverse modeling of nitrogen oxides emissions, *Atmos. Chem. Phys.*, *12*(24), 12,255–12,275.

Liu, Z., et al. (2010), Evidence of reactive aromatics as a major source of peroxy acetyl nitrate over China, *Environ. Sci. Technol.*, *44*(18), 7017–7022.

Liu, Z., et al. (2012a), Exploring the missing source of glyoxal (CHOCHO) over China, *Geophys. Res. Lett.*, *39*, L10812, doi:10.1029/2012GL051645.

Liu, Z., et al. (2012b), Summertime photochemistry during CAREBeijing-2007: RO_x budgets and O_3 formation, *Atmos. Chem. Phys.*, *12*(16), 7737–7752.

Ma, J. Z., A. Richter, J. P. Burrows, H. Nuss, and J. A. van Aardenne (2006), Comparison of model-simulated tropospheric NO_2 over China with GOME-satellite data, *Atmos. Environ.*, *40*(4), 593–604.

Martin, R. V., D. J. Jacob, K. Chance, T. P. Kurosu, P. I. Palmer, and M. J. Evans (2003), Global inventory of nitrogen oxide emissions constrained by space-based observations of NO_2 columns, *J. Geophys. Res.*, *108*(D17), 4537, doi:10.1029/2003JD003453.

Miyazaki, K., H. J. Eskes, and K. Sudo (2012), Global NO_x emission estimates derived from an assimilation of OMI tropospheric NO_2 columns, *Atmos. Chem. Phys.*, *12*(5), 2263–2288.

Ohara, T., H. Akimoto, J. Kurokawa, N. Horii, K. Yamaji, X. Yan, and T. Hayasaka (2007), An Asian emission inventory of anthropogenic emission sources for the period 1980–2020, *Atmos. Chem. Phys.*, *7*(16), 4419–4444.

Richter, A., V. Eyring, J. P. Burrows, H. Bovensmann, A. Lauer, B. Sierk, and P. J. Crutzen (2004), Satellite measurements of NO_2 from international shipping emissions, *Geophys. Res. Lett.*, *31*, L23110, doi:10.1029/2004GL020822.

Richter, A., J. P. Burrows, H. Nuss, C. Granier, and U. Niemeier (2005), Increase in tropospheric nitrogen dioxide over China observed from space, *Nature*, *437*(7055), 129–132.

Shi, C. N., H. J. S. Fernando, Z. F. Wang, X. Q. An, and Q. Z. Wu (2008), Tropospheric NO_2 columns over East Central China: Comparisons between SCIAMACHY measurements and nested CMAQ simulations, *Atmos. Environ.*, *42*(30), 7165–7173.

Stavrakou, T., J. F. Muller, K. F. Boersma, I. De Smedt, and R. J. van der A (2008), Assessing the distribution and growth rates of NO_x emission sources by inverting a 10-year record of NO_2 satellite columns, *Geophys. Res. Lett.*, *35*, L10801, doi:10.1029/2008GL033521.

Streets, D. G., et al. (2003), An inventory of gaseous and primary aerosol emissions in Asia in the year 2000, *J. Geophys. Res.*, *108*(D21), 8809, doi:10.1029/2002JD003093.

Uno, I., et al. (2007), Systematic analysis of interannual and seasonal variations of model-simulated tropospheric NO_2 in Asia and comparison with GOME-satellite data, *Atmos. Chem. Phys.*, *7*(6), 1671–1681.

van der A, R. J., D. Peters, H. Eskes, K. F. Boersma, M. Van Roozendael, I. De Smedt, and H. M. Kelder (2006), Detection of the trend and seasonal variation in tropospheric NO_2 over China, *J. Geophys. Res.*, *111*, D12317, doi:10.1029/2005JD006594.

Vinken, G. C. M., K. F. Boersma, A. van Donkelaar, and L. Zhang (2014), Constraints on ship NO_x emissions in Europe using GEOS-Chem and OMI satellite NO_2 observations, *Atmos. Chem. Phys.*, *14*(3), 1353–1369.

Wang, Y. H., Y. S. Choi, T. Zeng, B. Ridley, N. Blake, D. Blake, and F. Flocke (2006), Late-spring increase of trans-Pacific pollution transport in the upper troposphere, *Geophys. Res. Lett.*, *33*, L01811, doi:10.1029/2005GL024975.

Wang, Y., Y. Choi, T. Zeng, D. Davis, M. Buhr, L. G. Huey, and W. Neff (2007), Assessing the photochemical impact of snow NO_x emissions over Antarctica during ANTCI 2003, *Atmos. Environ.*, *41*(19), 3944–3958.

Yang, Q., Y. Wang, C. Zhao, W. Gustafson, and M. Shao (2011), NO_x emission reduction and its effects on ozone during the 2008 Olympic games, *Environ. Sci. Tech.*, *45*(4), 6404–6410.

Zeng, T., Y. H. Wang, K. Chance, E. V. Browell, B. A. Ridley, and E. L. Atlas (2003), Widespread persistent near-surface ozone depletion at northern high latitudes in spring, *Geophys. Res. Lett.*, *30*(24), 2298, doi:10.1029/2003GL018587.

Zeng, T., Y. Wang, K. Chance, N. Blake, D. Blake, and B. Ridley (2006), Halogen-driven low-altitude O_3 and hydrocarbon losses in spring at northern high latitudes, *J. Geophys. Res.*, *111*, D17313, doi:10.1029/2005JD006706.

Zhang, Q., et al. (2007), NO_x emission trends for China, 1995–2004: The view from the ground and the view from space, *J. Geophys. Res.*, *112*, D22306, doi:10.1029/2007JD008684.

Zhang, Q., et al. (2009), Asian emissions in 2006 for the NASA INTEX-B mission, *Atmos. Chem. Phys.*, *9*(14), 5131–5153.

Zhang, Q., G. N. Geng, S. W. Wang, A. Richter, and K. B. He (2012), Satellite remote sensing of changes in NO_x emissions over China during 1996–2010, *Chin. Sci. Bull.*, *57*(22), 2857–2864.

Zhao, C., and Y. Wang (2009), Assimilated inversion of NO_x emissions over east Asia using OMI NO_2 column measurements, *Geophys. Res. Lett.*, *36*, L06805, doi:10.1029/2008GL037123.

Zhao, C., Y. H. Wang, and T. Zeng (2009a), East China plains: A "basin" of ozone pollution, *Environ. Sci. Technol.*, *43*(6), 1911–1915.

Zhao, C., Y. Wang, Y. Choi, and T. Zeng (2009b), Summertime impact of convective transport and lightning NO_x production over North America: Modeling dependence on meteorological simulations, *Atmos. Chem. Phys.*, *9*(13), 4315–4327.

Zhao, C., Y. Wang, Q. Yang, R. Fu, D. Cunnold, and Y. Choi (2010), Impact of East Asian summer monsoon on the air quality over China: View from space, *J. Geophys. Res.*, *115*, D09301, doi:10.1029/2009JD012745.